Progress In Electromagnetics Research, Vol. 105, 273–294, 2010

COMPACT PATCH ANTENNA DESIGN FOR OUTDOOR RF ENERGY HARVESTING IN WIRELESS SENSOR NETWORKS

Z. W. Sim

Syngenta Sensors University Innovation Center
University of Manchester
UK

R. Shuttleworth

School of Electrical and Electronic Engineering
University of Manchester
UK

M. J. Alexander

National Physical Laboratory
Teddington, UK

B. D. Grieve

Syngenta Sensors University Innovation Center
University of Manchester
UK

Abstract—In this paper, two compact patch antenna designs for a new application — outdoor RF energy harvesting in powering a wireless soil sensor network — are presented. The first design is a low-profile folded shorted patch antenna (FSPA), with a small ground plane and wide impedance bandwidth. The second design is a novel FSPA structure with four pairs of slot embedded into its ground plane. Performance of both antennas was first simulated using CST Microwave Studio. Antenna prototypes were then fabricated and tested in the anechoic chamber and in their actual operating environment — an outdoor field. It was found that the FSPA with slotted ground plane achieved a comparable impedance bandwidth to the first design, with an overall size reduction of 29%. Simulations were

Corresponding author: Z. W. Sim (zhiwei.sim@postgrad.manchester.ac.uk).

also carried out to investigate the effects of different design parameters on the performance of the proposed slotted ground plane FSPA.

1. INTRODUCTION

In recent years, there has been a growing interest in the deployment of wireless sensor networks (WSN). These network systems, consisting of spatially distributed sensor nodes, are used extensively in a wide range of applications [1], such as structural monitoring [2], habitat monitoring [3], and healthcare systems [4, 5]. One emerging WSN application is in precision agriculture [6, 7], where sensor nodes are deployed in outdoor fields to monitor soil conditions, such as moisture, mineral content, and temperature. Information collected from these sensors can be used to manage irrigation, predict crop yield, and improve crop quality. Energy supply has been a key limiting factor to the lifetime of agricultural WSNs as their sensors are typically powered by onboard batteries which have fixed energy rating and limited lifespan. Therefore, these batteries need to be replaced in due time. Labor and maintenance costs can be prohibitive if the networks are deployed in hard-to-service locations. For instance, a wireless soil sensor which is buried underground has to be unearthed before the exhausted batteries can be replaced. Moreover, most wireless sensors batteries contain heavy metals, which can pollute the environment if improperly disposed of in landfill sites. A promising alternative to batteries is to use energy harvesting, in which ambient energy is captured, converted into electrical energy, and stored to power the wireless sensors. Several energy harvesting methods using different energy sources, such as light, temperature difference, electromagnetic field, human power, and mechanical vibration, have been reported in the literature [8, 9].

Selection of a feasible energy harvesting scheme for a specific application is mainly determined by two criteria: Operating environment and energy requirement of the wireless sensors. The main application envisaged for this work is a wireless soil sensor network deployed for in-field pest detection and monitoring [10]. In this particular network system, a number of wireless sensor nodes are distributed across an outdoor field surrounding a property, as depicted in Figure 1. These nodes are static at all times and can be located in an open area, in the shade of trees, or even covered by dried leaves or mud. Energy consumption of the soil sensor is approximately 29.4 J over 18 hours of operation.

Based on the given scenarios, a wireless power solution based

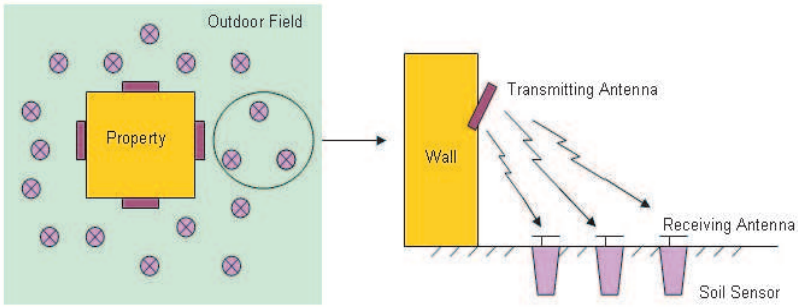

Figure 1. Wireless soil sensor network deployment architecture and RF energy transfer mechanism between the transmitting and receiving antennas.

on radio frequency (RF) energy harvesting is proposed. RF energy harvesting can not only be used to replenish the energy required for powering the sensors, but it can also provide a more controllable and predictable power supply compared to other energy harvesting methods. Using this technique, the RF energy radiated from a controlled transmitter is captured by a receiving antenna attached to each wireless sensor node. The received energy is converted into a DC voltage through a power conversion circuit. The DC energy is then stored in an energy storage device before being used to power the sensors.

In RF energy harvesting system, the receiving antenna is an important element as it is responsible for capturing energy from the nearby radiating sources. An appropriate receiving antenna design is imperative since the antenna characteristics, such as gain, radiation pattern, and impedance bandwidth, can affect the amount of harvestable energy. Microstrip patch antenna is an attractive candidate due to its low profile, low cost, and ease of fabrication. Over the years, many papers have been published on microstrip patch antennas for various applications, such as mobile communications [11–14], radio frequency identification (RFID) [15, 16], and medical telemetry [17]. In [11], a folded shorted patch antenna suitable for indoor mobile communication systems is presented. The design employs two contemporary techniques, namely folding the patch and using short circuit elements, to achieve dual resonance. The proposed antenna achieves a wide impedance bandwidth of 29.4% (1.48 to 1.99 GHz) at a low profile of $0.046\lambda_0$, where λ_0 is the free space wavelength at the center frequency of the impedance bandwidth. By cutting two slots in different parts of the patch, the antenna can be

further improved for dual-band operation [18]. The lower band has an impedance bandwidth of 21.1% (0.790 to 0.976 GHz) whereas the upper band attains an impedance bandwidth of 32.2% (1.698 to 2.350 GHz).

In this paper, we present further investigations on using the folded shorted patch antenna (FSPA) proposed in [11] as the receiving antenna for a new application — outdoor RF energy harvesting in powering a wireless soil sensor network. In [11], the antenna has a relatively large ground plane size ($0.92\lambda_0 \times 0.84\lambda_0$) which is not practical for the intended application. In our work, a much smaller ground plane size is implemented. In addition, a novel FSPA structure with slotted ground plane configuration [19–21] is also investigated. By incorporating slot pairs into its ground plane, the antenna is capable of meeting the desired bandwidth (860 to 960 MHz) at a much smaller overall size. Simulations are also performed to examine the effects of different design parameters on the performance of the slotted ground plane FSPA.

2. ANTENNA DESIGN REQUIREMENTS

2.1. Operating Frequency and Impedance Bandwidth

Selection of a proper operating frequency band for the proposed RF energy harvesting system is crucial since it will affect the overall size of the receiving antenna and operating range of the system. Two unlicensed UHF bands — 867 MHz and 2.45 GHz were evaluated. 867 MHz was chosen due to its lower free space attenuation (as the free space path loss at 2.45 GHz is about 9 dB higher than at 867 MHz). Table 1 shows the frequency allocation for the selected UHF band in various countries with its permitted radiated power level. For this system to be used worldwide, the receiving antenna has to be designed to resonate over a frequency range of 860 MHz to 960 MHz, with an impedance bandwidth ($S_{11} < -10$ dB) covering the chosen band.

Table 1. Frequency allocation and permitted radiated power level for the selected UHF band [22].

Country	Frequency Band	Power
United States	902–928 MHz	4 W E.I.R.P.
United Kingdom	865.6–867.6 MHz	2 W E.R.P./ 3.28 W E.I.R.P.
Japan	952–954 MHz	4 W E.I.R.P.

2.2. Antenna Size, Directivity, and Gain

It is desirable to keep the overall antenna size as small as possible so that it can be mounted easily upon the wireless sensor node. The overall size must also include the antenna's ground plane. A limitation of 20 mm antenna height from the soil surface has been imposed to protect the antenna from possible damage by agricultural equipment such as mowers and tractors. Since the antenna size can affect the maximum achievable gain and bandwidth [23], compromises need to be made in order to meet the design requirements. Moreover, the directivity of each receiving antenna is also important. As illustrated in Figure 1, the receiving antennas are raised slightly above the soil surface (instead of being buried) since the RF waves will experience additional attenuation when propagating through the soil [24]. In order to optimize the received energy, each receiver must be directed so that its main lobe is pointed towards the transmitter. An arbitrary benchmark minimum gain of 3 dBi was decided upon for the receiving antenna.

3. FOLDED SHORTED PATCH ANTENNA WITH NON-SLOTTED GROUND PLANE

3.1. Antenna Geometry

The geometry of the FSPA with non-slotted ground plane is shown in Figure 2. A rectangular patch is located in the middle of a square ground plane. Both patch and ground plane are made of copper sheet, which has a thickness of 1 mm. For the patch, one of its ends is shorted to ground while the other end is folded backwards. The patch structure is separated from the ground plane by an air layer. A coaxial feed and shorting post with the same diameter are positioned along the x-axis, which is the midline of the patch. In [11], the antenna is designed to cover frequencies between 1.48 and 1.99 GHz. Here, the patch dimension is modified so that the antenna can operate in the frequency band of 860 to 960 MHz. Besides, a much smaller ground plane is used for this antenna design. Assuming λ_0 is the free space wavelength of the center frequency at 910 MHz, the antenna has a ground plane dimension of 160 mm $(0.48\lambda_0) \times 160$ mm $(0.48\lambda_0)$, which is 70% less area than the ground plane proposed in [11, 18]. Detailed dimension of the antenna is shown in Table 2.

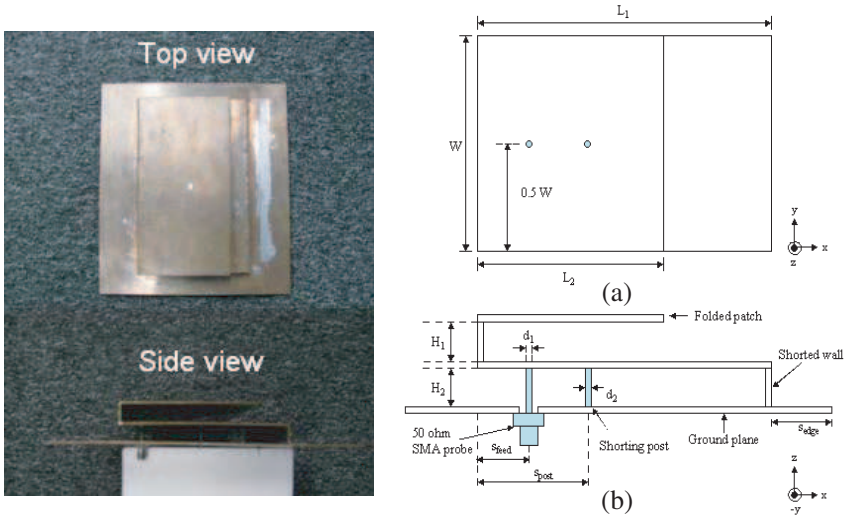

Figure 2. Geometry of the folded shorted patch antenna [11]. (a) Top view. (b) Side view.

Table 2. Antenna dimension.

Dimension	H_1	H_2	W	L_1	L_2
(mm)	8.0	8.0	125.0	90.0	73.0
Dimension	Spost	Sfeed	Sedge	d_1	d_2
(mm)	7.5	47.5	35.0	1.3	1.3

3.2. Simulation and Measurement Results

The FSPA with non-slotted ground plane was first simulated using CST Microwave Studio. In order to validate the simulation results, the antenna was fabricated and tested. The return loss was measured by an Agilent HP5071B Network Analyzer while the gain radiation patterns were obtained in the SMART chamber of the National Physical Laboratory (NPL) and the anechoic chamber of University of Manchester.

3.2.1. Return Loss

Figure 3 shows the simulated and measured return losses of the antenna. It is seen that the antenna has two resonances close to each other, which results in a wider impedance bandwidth. The simulated and measured impedance bandwidths ($S_{11} < -10$ dB) are 17.8% (0.834 to 0.997 GHz) and 20.0% (0.815 to 0.997 GHz), respectively.

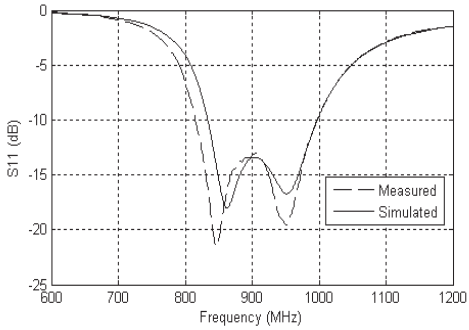

Figure 3. Measured and simulated return loss of the FSPA with non-slotted ground plane (160 mm × 160 mm).

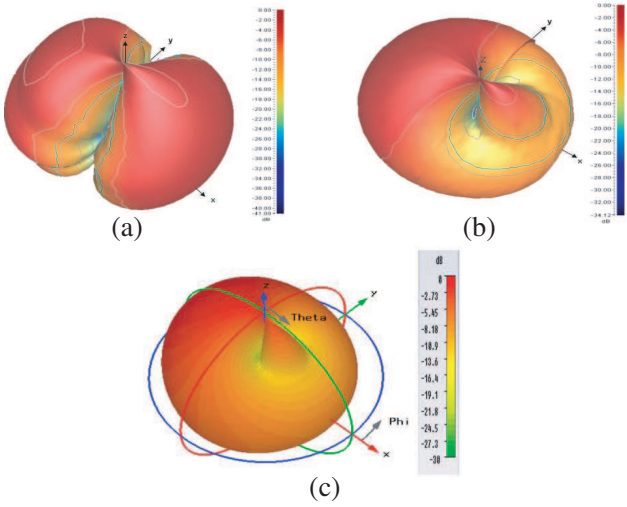

Figure 4. 3-D co-polar radiation pattern of the FSPA with non-slotted ground plane at 867 MHz using. (a) Cable measurement, (b) optical fiber measurement, and (c) CST simulation.

3.2.2. Radiation Pattern and Gain

The 3-D radiation pattern and gain of the antenna was measured in the SMART Chamber of NPL [25]. For this measurement, the antenna was connected with either a coaxial cable or an optical fiber via an opto-electric field sensor (OEFS) transducer [25], to a HP 8510 network analyzer. An EMCO 3147 log periodic antenna was used as the transmit antenna. Figure 4 compares the measured 3-D radiation pattern at 867 MHz using cable versus using optical fiber

with the simulated pattern obtained from CST. In Figure 4(a), nulls can be seen in the plot with the coaxial cable; these are caused by destructive interference of radiation from the cable due to common mode currents from the antenna. The unwanted influence of common mode currents distorts the overall radiation pattern. The plot for the optical transducer and fiber connection shown in Figure 4(b) has a better radiation pattern and it matches closer to the simulated pattern in Figure 4(c). The co-polar x-z plane radiation patterns at 867 MHz, 915 MHz, and 953 MHz, are displayed in Figure 5. The main beams are tilted to $-35°$ at 867 MHz, $-18°$ at 915 MHz, and $-10°$ at 953 MHz. The co-polar y-z plane radiation patterns are also shown in Figure 6. In y-z plane, the main beams are in the broadside direction of the antenna. The measured peak gains (of x-z plane) at 867 MHz, 915 MHz, and 953 MHz, are 3.9 dBi, 5.9 dBi and 6.3 dBi, respectively.

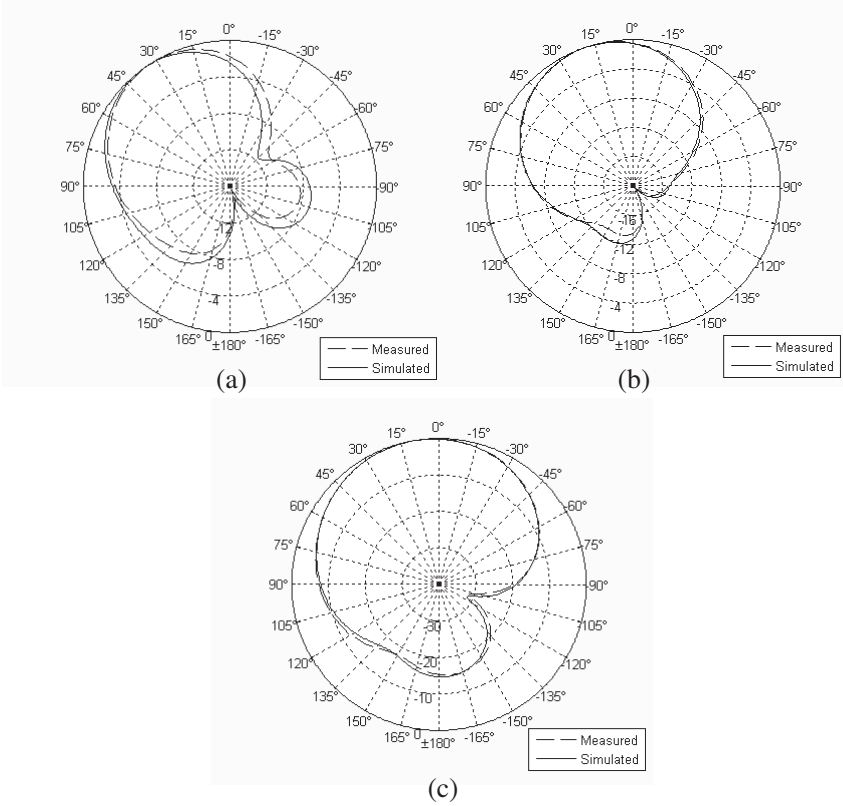

Figure 5. Measured and simulated radiation pattern of the FSPA (co-polar x-z plane). (a) 867 MHz. (b) 915 MHz. (c) 953 MHz.

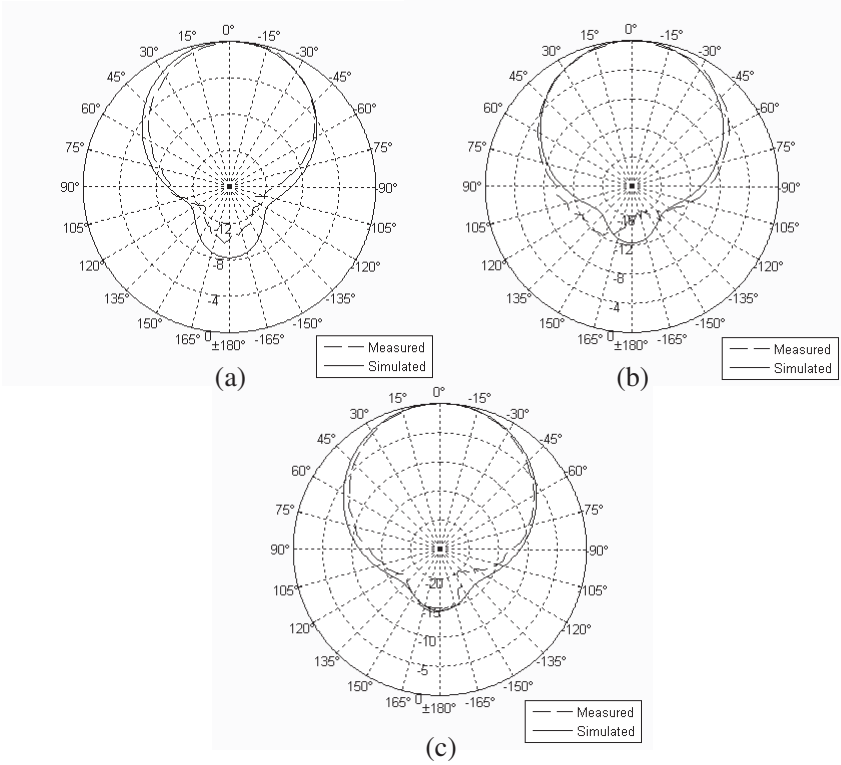

Figure 6. Measured and simulated radiation pattern of the FSPA (co-polar y-z plane). (a) 867 MHz. (b) 915 MHz. (c) 953 MHz.

4. FOLDED SHORTED PATCH ANTENNA WITH SLOTTED GROUND PLANE

4.1. Antenna Geometry

In this section, a new FSPA structure with slotted ground plane and reduced overall size is presented. The geometry of this antenna is almost identical to Figure 2 with the exception of its slotted ground plane configuration. Four pairs of equally spaced slots are embedded into the ground plane, as illustrated in Figure 7. Each slot has the same width (W_s) and length (L_s). The slot pairs are spaced by the same distance (S_1). The slotted ground plane has a dimension of 135 mm × 135 mm, which is smaller than that of FSPA described in Section 3. Detailed dimension of the antenna is given in Table 3.

Table 3. Antenna dimension.

Patch					
Dimension	H_1	H_2	W	L_1	L_2
(mm)	10.0	6.0	90.0	90.0	72.0
Dimension	Spost	Sfeed	Sedge	d_1	d_2
(mm)	32.5	7.5	22.5	1.3	1.3

Ground Plane					
Dimension	W_g	L_g	L_s	W_s	S_1
(mm)	135.0	135.0	58.0	6.0	25.0
Dimension		S_2	G_1	G_2	
(mm)		10.0	14.5	39.5	

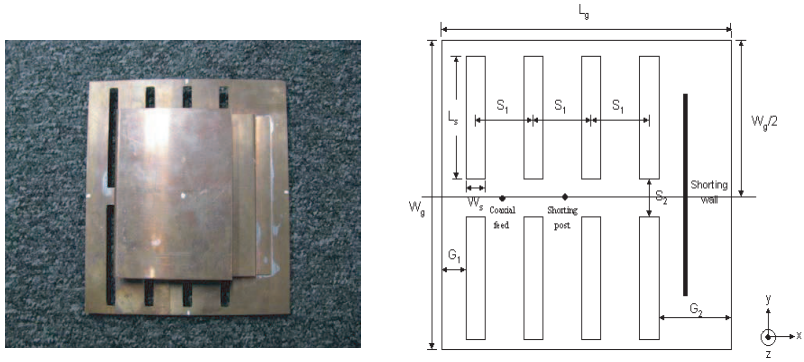

Figure 7. Geometry of the slotted ground plane.

4.2. Simulation and Measurement Results

4.2.1. Return Loss

Figure 8 compares the simulated and measured return losses of the antenna. The simulated and measured impedance bandwidths ($S_{11} < -10\,\text{dB}$) are 18.3% (0.835 to 1.003 GHz) and 18.7% (0.834 to 1.006 GHz), respectively.

4.2.2. Radiation Pattern and Gain

The simulated and measured co-polar x-z plane radiation patterns of the antenna at 867 MHz, 915 MHz, and 953 MHz, are shown in Figure 9. Good agreement between simulation and measurement results is observed. The main beams are tilted at $-24°$ at 867 MHz,

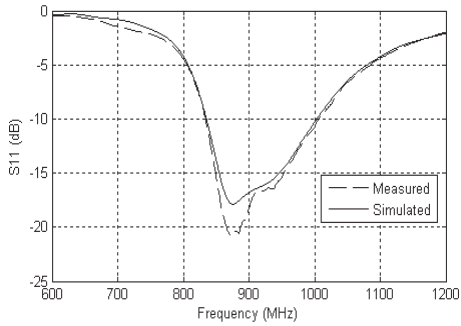

Figure 8. Measured and simulated return loss of the folded shorted patch antenna with slotted ground plane (135 mm × 135 mm).

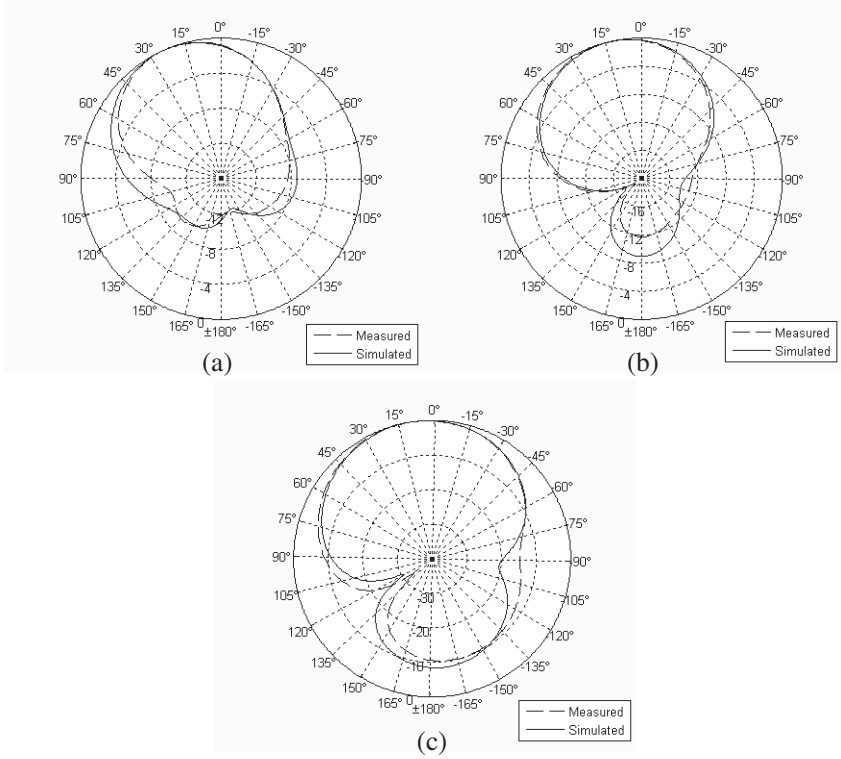

Figure 9. Measured and simulated co-polar x-z plane radiation pattern of the FSPA with slotted ground plane at (a) 867 MHz, (b) 915 MHz, and (c) 953 MHz.

-13° at 915 MHz, and -9° at 953 MHz. The co-polar y-z plane radiation patterns of this antenna are similar to the patterns shown in Figure 6. For brevity, we do not show the patterns here. The measured peak gains (of x-z plane) at 867 MHz, 915 MHz, and 953 MHz, are 3.8 dBi, 5.4 dBi and 5.8 dBi, respectively.

By comparing the simulation results of this antenna to the FSPA with non slotted ground plane (Section 3), it can be seen that the two antennas have a comparable impedance bandwidth with similar gain performance. However, the FSPA with slotted ground plane has a much smaller patch and ground plane dimension. An overall size reduction of 29% is achieved by the FSPA when slots are properly embedded in the ground plane.

4.3. Effect of the Slotted Ground Plane

To thoroughly understand the effect of the slots, we simulated the proposed FSPA using a non-slotted ground plane, having an identical area of 135 mm × 135 mm. Figure 10 shows the simulated input impedance against frequency curves of the FSPA with and without the slotted ground plane. From Figure 10(b), it is seen that the input reactance of the antenna with non-slotted ground plane at frequency band of interest (860–960 MHz) is dominated by inductive reactance, which is mainly from the probe feed. By incorporating slot pairs into the ground plane, additional capacitive reactance is introduced to counteract the inductive reactance, providing better impedance matching across the band. Figure 11 compares the simulated return losses of the two prototypes. The FSPA with slotted ground plane has a bandwidth of 18.4% while the FSPA with non-slotted ground plane does not match to 50 Ω.

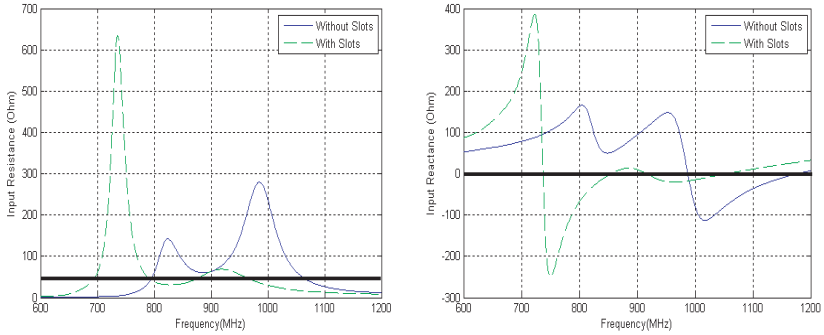

Figure 10. Simulated input impedance of the FSPA with and without slotted ground plane. (a) Resistance and (b) reactance.

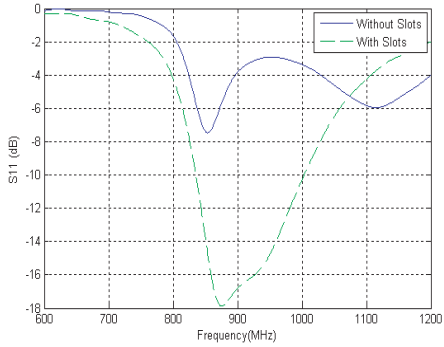

Figure 11. Simulated return loss of FSPA with and without slotted ground plane.

5. PARAMETRIC ANALYSES

In order to examine the effects of different design parameters on the impedance bandwidth and radiation patterns of the FSPA with slotted ground plane, parametric analyses are performed using CST Microwave Studio. Simulations were carried out by varying the chosen parameter whilst keeping all other parameters constant. Initial dimensions of the investigated parameters are shown in Table 3. First, three parameters characterizing the slots of the ground plane — number of slot pairs, slot length, and slot width, were investigated. The effects of slot pairs (labeled from A to E shown in Figure 12) on the antenna's impedance bandwidth are depicted in Figure 13. As the number of slot pairs increases, the FSPA achieves a wider impedance bandwidth. The widest bandwidth is achieved when four pairs of slot (A, B, C and D) are used. The addition of Pair E does not change the antenna's bandwidth performance. Figures 14 and 15 demonstrate the effects of slot length and width. In most cases, the impedance bandwidth becomes wider with the increments of slot length and width. However, no further improvement is found for the case where the slot width is more than 4 mm. We observed that changing the number of slot pairs and the dimension of slot have no significant effect on the antenna radiation patterns (directivity and tilted angle of the main lobe).

We also investigated five other design parameters related to the patch structure — folded patch width (W), folded patch length (L_2), height ratio (H_1/H_2), position of the shorting post (s_{post}), and location of the probe feed (s_{feed}). The effect of each parameter on the FSPA's impedance bandwidth and radiation patterns are displayed in Figures 16 to 18, Tables 4 and 5, respectively. By increasing W,

L_2, and H_1/H_2 up to a certain value, wider impedance bandwidth can be obtained. It is worth noting that the locations of the probe feed and shorting pin can also be adjusted to provide better tuning of impedance matching, as shown in Figures 17 and 18. Meanwhile, increasing L_2 and H_1/H_2 results in higher antenna directivity but with a smaller tilted angle of the main lobe from the broadside direction, which is undesired for the intended application. Hence, a tradeoff must be made when selecting the design parameters of the FSPA. Changes in W, S_{post}, and S_{feed} have no significant effect on the antenna radiation patterns.

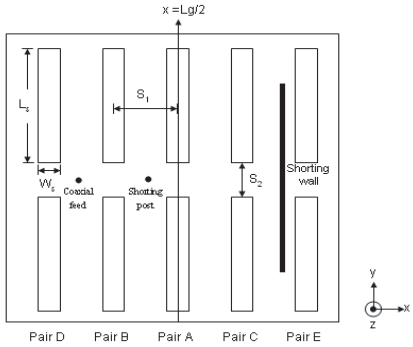

Figure 12. Slot pair A to E.

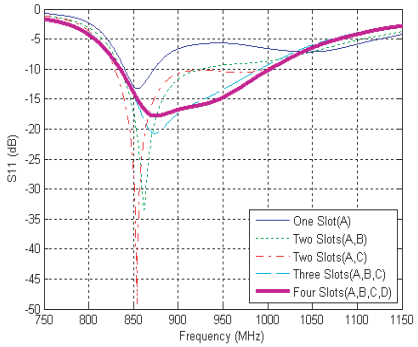

Figure 13. Simulated return losses for different number pair of slots.

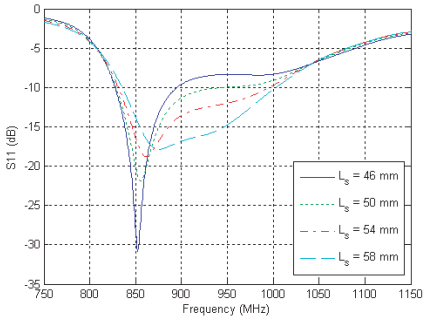

Figure 14. Simulated return losses for various L_s.

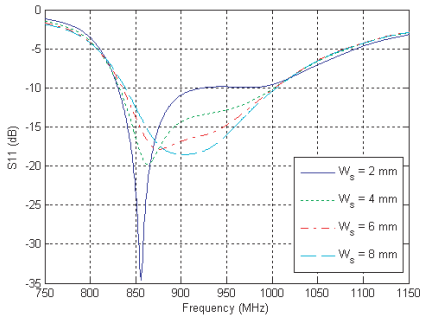

Figure 15. Simulated return losses for various W_s.

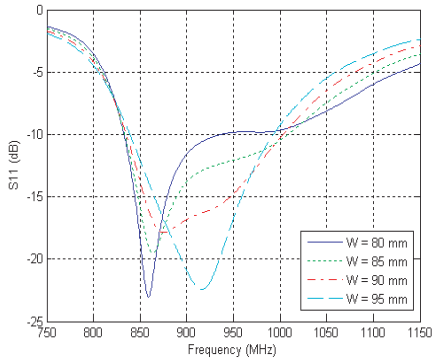

Figure 16. Simulated return losses for various W.

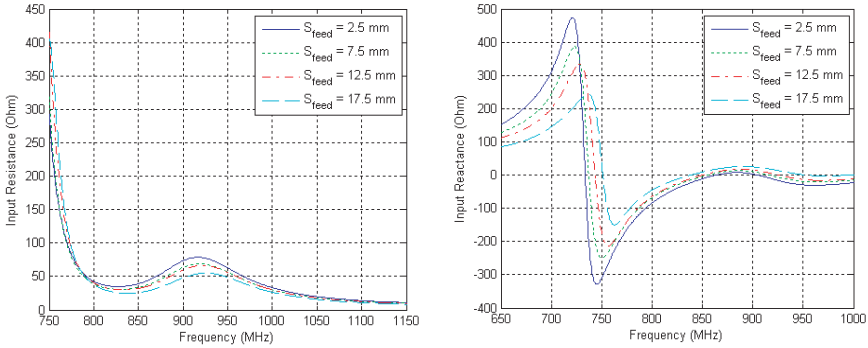

(a) (b)

Figure 17. Simulated input impedance of the FSPA for various S_{feed}.

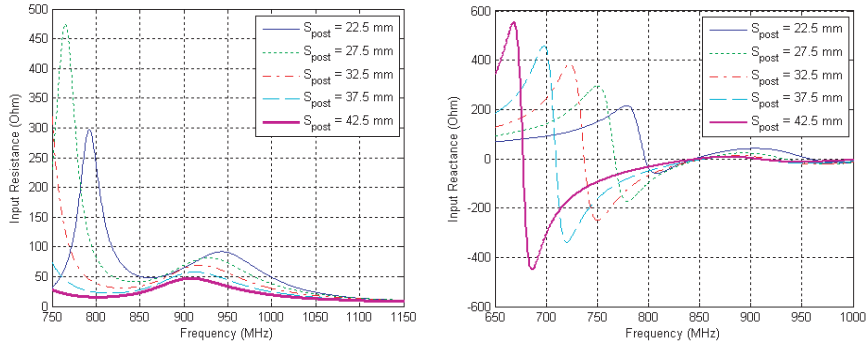

(a) (b)

Figure 18. Simulated input impedance of the FSPA for various S_{post}.

Table 4. Simulated antenna performance for various L_2.

Parameter	Return Loss	Radiation Pattern		
Folded Patch Length (L_2)	**Impedance Bandwidth ($S_{11} < -10$ dB)**	**Center Frequency**	**Tilted Angle of Main Lobe (x-z plane)**	**Maximum Directivity (dBi)**
68 mm	0.888–1.040 GHz (15.8%)	867 MHz	45°	3.0
		915 MHz	24°	4.8
		953 MHz	15°	5.7
70 mm	0.858–1.023 GHz (17.5%)	867 MHz	34°	3.8
		915 MHz	17°	5.4
		953 MHz	12°	6.0
72 mm	0.835–1.003 GHz (18.3%)	867 MHz	24°	4.4
		915 MHz	13°	5.8
		953 MHz	6°	6.2
74 mm	0.816–0.980 GHz (18.2%)	867 MHz	17°	5.2
		915 MHz	10°	6.0
		953 MHz	7°	6.2
76 mm	0.799–0.925 GHz (14.6%)	867 MHz	13°	5.6
		915 MHz	8°	6.1
		953 MHz	6°	6.2

6. FIELD TRIAL EXPERIMENTAL RESULTS

To evaluate the performance of both FSPAs in their actual operating environment, an outdoor field trial was conducted in a farm area located at Huddersfield, UK. The experimental setup is shown in Figure 19. A mobile radio manufactured by Tait Electronic Ltd. was used as the radiating source. The radio was programmed to transmit at 867.0 MHz with an output power of 33 dBm (2 W), and fed to a vertically polarized patch antenna made by Wilson Electronics, through a 3-dB attenuator and coaxial cables. The transmit antenna has a measured peak gain of 5.2 dBi at 867.0 MHz. The attenuator loss, cable loss, and return loss between the radio and the antenna were measured to be around 3.5 dB. Hence, the maximum radiated power of this transmitter system is about 34.7 dBm (3W EIRP), which is within the permitted radiated power given in Table 1. At the receiving end, both FSPAs with non-slotted (Section 3) and slotted ground plane (Section 4) were deployed as the receiving antennas. The two antennas were placed on a turf with short grass, as seen in Figure 20.

Table 5. Simulated antenna performance for various H_1/H_2.

Parameter	Return Loss	Radiation Pattern		
Antenna Height (H_1/H_2)	**Impedance Bandwidth ($S_{11} < -10$ dB)**	**Center Frequency**	**Tilted Angle of Main Lobe (x-z plane)**	**Maximum Directivity (dBi)**
12 mm/ 4 mm	0.816– 1.040 GHz (16.5%)	867 MHz	18°	5.2
		915 MHz	11°	5.9
		953 MHz	7°	6.1
10 mm/ 6 mm	0.835– 1.003 GHz (18.2%)	867 MHz	24°	4.4
		915 MHz	13°	5.8
		953 MHz	6°	6.2
8 mm/ 8 mm	0.856– 1.041 GHz (19.5%)	867 MHz	39°	3.3
		915 MHz	17°	5.5
		953 MHz	11°	6.1
6 mm/ 12 mm	0.882– 1.069 GHz (19.2%)	867 MHz	61°	1.9
		915 MHz	29°	4.3
		953 MHz	14°	5.9

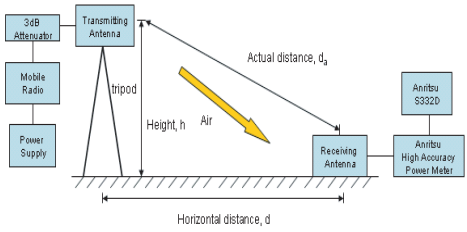

Figure 19. Experimental setup of the field trial.

Figure 20. Field trial at Huddersfield.

First, the return losses of both antennas were measured using an Anritsu S332D Site Master™ Cable and Antenna Analyzer. As shown in Figures 21 and 22, the return loss and impedance characteristic of the antennas change marginally when placed on the turf due to the underlying soil having variable dielectric constant and electrical conductivity [26]. However, S_{11} of the two antennas remained below -10 dB across 860 to 960 MHz band. Their impedance bandwidths improved slightly compared to that of the free space test. The

received power of each FSPA was also measured using an Anritsu High Accuracy Power Meter (PSN50), connected to the tested FSPA using RF coaxial connectors and cables. Losses of these connectors and cables were measured at 0.70 dB at 867.0 MHz. To determine the actual received power of the antenna, losses were taken into account during the measurements. The transmit antenna was mounted on a tripod set to provide three different heights of 0.70 m, 1.00 m, and 1.45 m. Meanwhile, the receiving antennas were located on the turf with their main radiating edge facing towards the transmitter. Both transmitting and receiving antennas were aligned to have the same polarization. By manually adjusting the transmit antenna towards the FSPA, the peak received power was recorded.

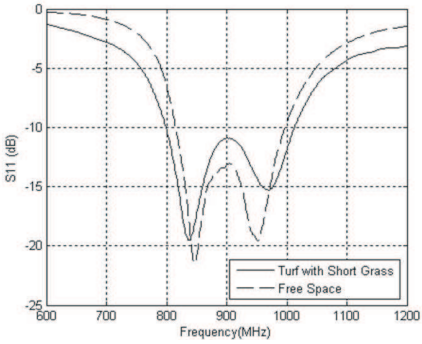

Figure 21. Measured return loss of FSPA with non-slotted ground plane on turf and free space.

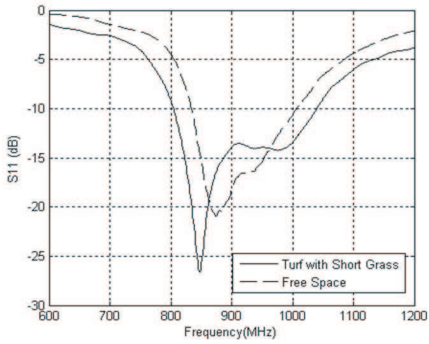

Figure 22. Measured return loss of FSPA with slotted ground plane on turf and free space.

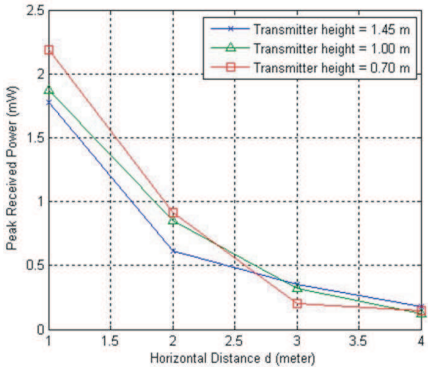

Figure 23. Measured peak received power of FSPA with non-slotted ground plane (FSPA1).

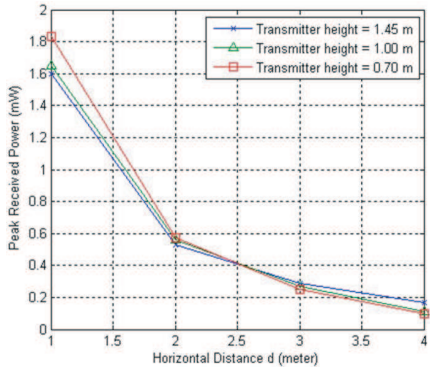

Figure 24. Measured peak received power of FSPA with slotted ground plane (FSPA2).

Figures 23 and 24 show the measured peak received power of both FSPAs with non-slotted ground plane (FSPA1) and slotted ground plane (FSPA2). At $h = 1.45$ meters and $d = 2$ meters, the peak received power of FSPA1 and FSPA2 were measured as 0.61 mW and 0.53 mW, respectively. Although both antennas have a comparable measured peak gain at 867 MHz (as discussed in Section 4), FSPA2 receives less power since it has a smaller patch dimension, which results in a smaller energy collection area. It is also observed that the received power of both antennas increases when the transmitter height is lowered. This is because the actual distance between transmitter and receiver decreases when lowering the transmitter. However, this observation does not hold true at a horizontal distance more than 2 meters, since at a lower transmitter height; part of the radiated energy from the main beam may not be captured due to the directional nature of the receiving antenna.

7. CONCLUSION

This paper presents simulated and experimental investigations of using two folded shorted patch antennas (FSPA) for a new application — outdoor RF energy harvesting in powering a wireless soil sensor network. A novel FSPA structure with slotted ground plane configuration was introduced and studied. By properly embedding slot pairs into the ground plane, the FSPA can achieve comparable impedance bandwidth and gain performance to a conventional FSPA (with non-slotted ground plane), at an overall size reduction of 29%. Both antennas (with and without slotted ground plane) meet the required bandwidth specification of 860 to 960 MHz and have peak gains of more than 3 dBi across the operating band. In addition, the proposed antennas are low profile (with antenna height less than 20 mm) and easy to fabricate, making them very suitable for the intended application. An outdoor field trial was also conducted to verify the performance of the FSPAs in their actual operating environment. The collected data from the trial provides useful information towards the power conversion circuit design of the proposed energy harvesting system.

ACKNOWLEDGMENT

The authors wish to acknowledge their appreciation to National Physical Laboratory (NPL) for loaning the SMART chamber for antenna measurements.

REFERENCES

1. Akyildiz, I. F., W. Su, Y. Sankarasubramaniam, and E. Cayirci, "Wireless sensor networks: A survey," *Computer Networks*, Vol. 38, 393–422, 2002.
2. Ning, X., R. Sumit, C. Krishna Kant, G. Deepak, B. Alan, G. Ramesh, and E. Deborah, "A wireless sensor network for structural monitoring," *Proceedings of the 2nd International Conference on Embedded Networked Sensor Systems*, Baltimore, USA, 2004.
3. Alan, M., C. David, P. Joseph, S. Robert, and A. John, "Wireless sensor networks for habitat monitoring," *Proceedings of the 1st ACM International Workshop on Wireless Sensor Networks and Applications*, Atlanta, USA, 2002.
4. Dobrescu, R., M. Dobrescu, D. Popescu, and H. G. Coanda, "Embedded wireless homecare monitoring system," *International Conference on eHealth, Telemedicine, and Social Medicine*, 66–71, 2009.
5. Virone, G., A. Wood, L. Selavo, Q. Cao, L. Fang, T. Doan, Z. He, and J. Stankovic, "An advanced wireless sensor network for health monitoring," *Transdisciplinary Conference on Distributed Diagnosis and Home Healthcare*, April 2006.
6. Baggio, A., "Wireless sensor networks in precision agriculture," *ACM Workshop Real-World Wireless Sensor Networks*, 2005.
7. John, M., M. Paul, G. Siddeswara Mayura, P. Wei, H. Daniel, and T. Andrew, "Wireless sensor network deployment for water use efficiency in irrigation," *Proceedings of the Workshop on Real-world Wireless Sensor Networks*, Glasgow, Scotland, 2008.
8. Paradiso, J. A. and T. Starner, "Energy scavenging for mobile and wireless electronics," *IEEE Pervasive Computing*, Vol. 4, 18–27, January–March 2005.
9. Thomas, J. P., M. A. Qidwai, and J. C. Kellogg, "Energy scavenging for small-scale unmanned systems," *Journal of Power Sources*, Vol. 159, 1494–1509, 2006.
10. Wright, P., P. R. Green, B. D. Grieve, T. A. York, and M. Hoppe, "Automated termite sensing," *IEEE Sensors Applications Symposium*, 99–104, 2009.
11. Li, P., K. L. Lau, and K. M. Luk, "Wideband folded shorted patch antenna with low profile," *IEEE Electronics Letters*, Vol. 41, 112–113, 2005.
12. Mak, C. L., H. Wong, and K.-M. Luk, "High-gain and wide-band single-layer patch antenna for wireless communications," *IEEE*

Transactions on Vehicular Technology, Vol. 54, 33–40, 2005.

13. Islam, M. T., M. N. Shakib, and N. Misran, "Broadband E-H shaped microstrip patch antenna for wireless systems," *Progress In Electromagnetics Research*, Vol. 98, 163–173, 2009.
14. Secmen, M. and A. Hizal, "A dual-polarized wide-band patch antenna for indoor mobile communication applications," *Progress In Electromagnetics Research*, Vol. 100, 189–200, 2010.
15. Budak, E., B. Catay, I. Tekin, H. Yenigun, M. Abbak, and S. Drannikov, "Microstrip patch antenna for RFID applications," *1st Annual RFID Eurasia*, 1–3, 2007.
16. Lin, P.-J., H.-C. Teng, Y.-J. Huang, and M.-K. Chen, "Design of patch antenna for RFID reader applications," *International Conference on Anti-counterfeiting, Security, and Identification in Communication*, 193–196, 2009.
17. Chandran, A. R., G. A. Conway, and W. G. Scanlon, "Compact low-profile patch antenna for medical body area networks at 868 MHz," *Antennas and Propagation Society International Symposium*, 1–4, 2008.
18. Lau, K. L., K. C. Kong, and K. M. Luk, "A miniature folded shorted patch antenna for dual-band operation," *IEEE Transactions on Antennas and Propagation*, Vol. 55, 2391–2398, 2007.
19. Sim, C.-Y.-D. and T.-Y. Han, "GPS antenna design with slotted ground plane," *Microwave and Optical Technology Letters*, Vol. 50, 818–821, 2008.
20. Soliman, A. S., A. A. Esmat, and A.-A. Darwish, "Slotted ground plane of rectangular patch microstrip antenna with enhanced bandwidth and size reduction," *Proceedings of the 12th WSEAS International Conference on Communications*, Heraklion, Greece, 2008.
21. Chiou, T.-W. and K.-L. Wong, "Designs of compact microstrip antennas with a slotted ground plane," *IEEE Antennas and Propagation Society International Symposium*, Vol. 2, 732–735, 2001.
22. Brown, D., *RFID Implementation*, McGraw-Hill Professional, 2006.
23. Harrington, R. F., "Effect of antenna size on gain, bandwidth, and efficiency," *J. Res. Nat. Bureau Standards*, Vol. 64D, 1–12, January–February 1960.
24. Akyildiz, I. F. and E. P. Stuntebeck, "Wireless underground sensor networks: Research challenges," *Ad Hoc Networks*, Vol. 4,

669–686, 2006.

25. Loh, T. H., M. Alexander, F. Widmer, P. Miller, and D. Knight, "Validation of a new small-antenna radiated testing range," *3rd European Conference on Antennas and Propagation*, 699–703, Berlin, Germany, March 2009.
26. Lee, W. C. Y., *Mobile Communications Engineering*, McGraw-Hill, 1982.